ARCHIVES OF METALLURGY AND MATERIALS
Volume 51 2006 Issue 4

L. LITYŃSKA-DOBRZYŃSKA*

EFFECT OF HEAT TREATMENT ON THE SEQUENCE OF PHASES FORMATION IN Al-Mg-Si ALLOY WITH Sc AND Zr ADDITIONS

WPŁYW OBRÓBKI CIEPLNEJ NA SEKWENCJĘ FAZ TWORZĄCYCH SIĘ W STOPACH Al-Mg-Si Z DODATKAMI Sc I Zr

In the present work the sequence of phases in Al-1%Mg-0.6%Si (in wt %) alloys with 0.4%Sc and 0.2%Zr additions during heat treatment has been studied. The investigated alloys were cast into copper mould to ensure high cooling rate during solidification and the retention of Sc and Zr in the supersaturated solid solution. Two step preliminary heat treatment was applied: the annealing in temperature 300°C or 350°C followed by quenching from 540°C to water. The precipitation of the β'' (Mg_2Si), cubic β (Mg_2Si) and $Al_3(Sc, Zr)$ phases has been observed during the first step of annealing. The annealing at 540°C has led to complete dissolution of the Mg_2Si particles and growth of the spherical particles of the $Al_3(Sc, Zr)$ phase. The increase of hardness during subsequent ageing at 165°C (typical ageing temperature of the 6xxx type alloys) has been caused by the formation of needle-like β'' phase which coexist with $Al_3(Sc, Zr)$ precipitates.

Keywords: Al-Mg-Si, Al_3Sc, $Al_3(Sc, Zr)$, precipitation, TEM

W pracy przebadano wpływ obróbki cieplnej na sekwencję faz tworzących się w stopach Al-1%Mg-0.6%Si zawierających 0.4%Sc i 0.2%Zr (% wag.). Stopy odlewano do grubościennej kokili miedzianej zapewniającej duże szybkości krzepnięcia oraz zatrzymanie Sc i Zr w roztworze stałym aluminium. Zastosowano dwustopniową wstępną obróbkę cieplną: wygrzewanie w 300°C lub 350°C oraz przesycanie z 540°C do wody. W pierwszym etapie obróbki cieplnej wydzielały się następujące fazy: β'', kubiczna $\beta(Mg_2Si)$ oraz $Al_3(Sc, Zr)$. Podczas wygrzewania w temperaturze 540°C zachodzi całkowite rozpuszczenie wydzieleń typu Mg_2Si i wzrost sferycznych wydzieleń fazy $Al_3(Sc, Zr)$. Wzrost twardości stopów podczas starzenie w temperaturze 165°C (jest to typowa temperatura starzenia stopów serii 6000) spowodowany jest obecnością igłowych wydzieleń metastabilnej fazy β'', które towarzyszą wydzieleniom $Al_3(Sc, Zr)$.

1. Introduction

The 6xxx series alloys based on Al-Mg-Si are widely used as medium-strength, corrosion-resistant materials. The alloys are age hardenable and the decomposition of the supersaturated alloys depends on the alloy composition and the heat treatment. The phases precipitating in Al-Mg_2Si quasi-binary alloys have been reported as needle shaped β'' with a monoclinic structure, rod shaped hexagonal β' (both phases are metastable) and cubic β (Mg_2Si) equilibrium phase [1-3].

The addition of a small amount of scandium to aluminum alloys can improve their properties, such as strength, heat resistance, welding characteristics, grain size etc. [4, 5]. The beneficial role of scandium is attributed to a high density of coherent precipitates of the Al_3Sc phase ($L1_2$ structure) formed during decomposition of the solid solution at temperatures between 300-550°C [6-8]. Alloying with zirconium in addition to scandium improves both the grain-refining efficiency and thermal stability of the alloys [9]. However, in the multicomponent aluminum alloys the Sc efficiency depends on the type of interaction with other alloying elements and on the phase and structural transformations during ageing. Ternary phase diagrams of Al-Mg-Sc and Al-Si-Sc presented in Figure 1 show the phases being in equilibrium with the aluminum solid solution. No ternary AlMgSc phases were observed, while in the Al-Si-Sc system the Al_3Sc phase coexist with the ternary tetragonal $AlSi_2Sc_2$ phase (a = 0.6597 nm, c = 0.3994), named V-phase, above 0.25 wt% of Si. The particles of the V-phase does not participate in strengthening of the al-

* INSTITUTE OF METALLURGY AND MATERIALS SCIENCE, POLISH ACADEMY OF SCIENCES, 30-059 KRAKÓW, 25 REYMONTA STR., POLAND

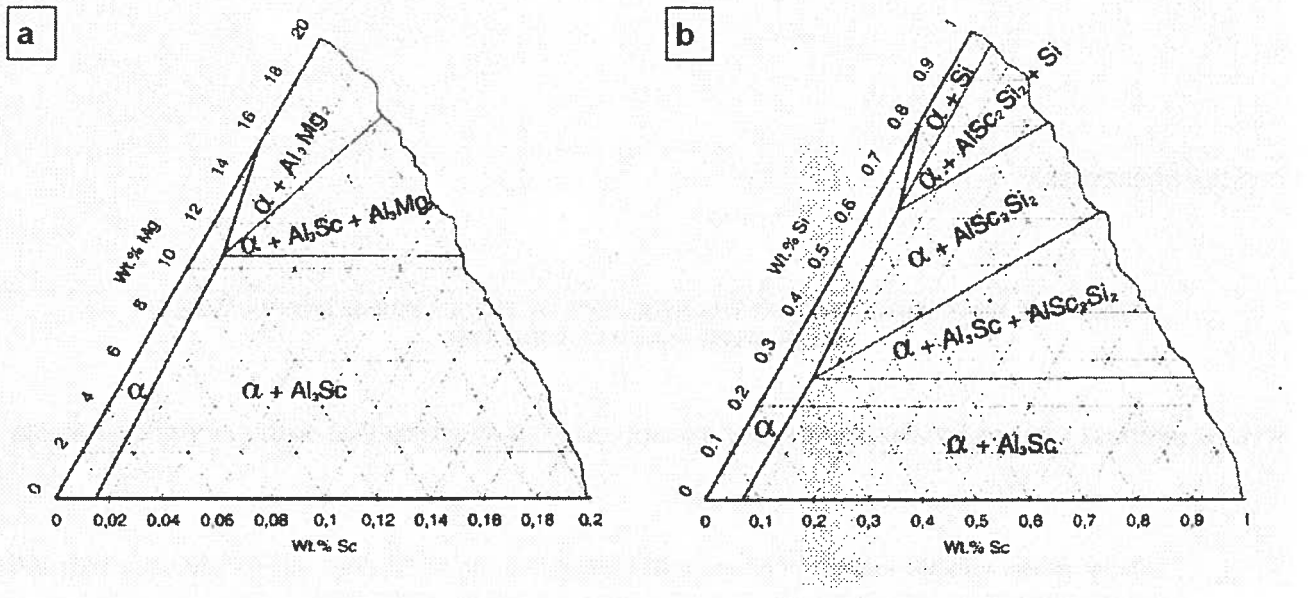

Fig. 1. Isothermal section of Al corner of (a) Al-Sc-Mg phase diagram at 430°C and (b) Al-Sc-Si phase diagram at 500°C [5]

loy removes scandium from the solid solution and reduces the positive effect of Al_3Sc precipitates. However, it has been reported that Sc and Zr additions to Al-Mg-Si alloys reduce the grain size in as-cast alloys and cause the formation of a fine-scaled and stable non-recrystallized microstructure [10, 11]. The hardness of Al-Mg-Si increases with Sc or Sc+Zr additions after annealing at temperatures between 300-540°C as well as during ageing at 165°C [11].

The objective of the present study is to characterize the precipitation sequences of the phases during heat treatment in Al-Mg-Si alloys with Sc and Sc + Zr additions.

2. Experimental

The alloys of nominal composition (in wt.%) Al-1.0 Mg-0.6 Si-0.4 Sc (alloy A) and Al-1.0 Mg-0.6 Si-0.4 Sc-0.2 Zr (alloy B) were prepared using Al-2 wt.% Sc, Al-45 wt.% Si, Al-10 wt.% Zr master alloys and high-purity Mg (99.99%) and Al (99.99%). The contents of Mg and Si were balanced to obtain the Mg/Si ratio of 1.73:1 (corresponding to the 2:1 stoichiometry for Mg_2Si phase). After melting, the alloys were cast into a thick-walled copper mould to ensure a high cooling rate during solidification, which is necessary for the retention of Sc and Zr in supersaturated solid solution. The ingots had dimensions of 15×6×1.5 cm. The cast alloys were annealed at 300°C or 350°C (these temperatures correspond to the effective start of the precipitation of the Al_3Sc, $Al_3(Sc, Zr)$ phases, respectively). Subsequently, the alloys were annealed at 540°C for 30 min to dissolve the Mg_2Si eutectic phase formed during casting and the Mg_2Si formed during the first step of annealing. After a quench in water, further ageing was performed at 165°C (optimal ageing temperature of 6000 type alloys). The microstructure of cast and thermal treated alloys was examined using Leica DM IRM optical microscope, scanning electron microscope Philips XL30 and analytical transmission electron microscope Philips CM20 operating at 200 kV equipped with EDAX X-ray detector. The Fischione double jet electropolisher was used for thin foil preparation in electrolyte containing nitric acid and methanol (1:3), at a temperature of – 30°C and a voltage of 15 V.

3. Results

Figure 2 shows typical microstructures of the as cast alloys. Alloy A consists of large columnar grains (200-500 μm) near the walls of the mould and smaller (100-300 μm), equiaxed grains at the centre of the ingot (Fig. 2a, b). Dendritic sub-structure is visible within the grains in the both areas. In alloy B fine equiaxed grain structure, with the grain size about 100 μm, was observed in the whole volume of the cast billet (Fig. 2c, d).

SEM image of the as cast alloy B is presented in Fig. 3. Energy dispersive X-ray (EDX) microanalysis allowed to identify the phases, situated in the grain boundary. The dark phase was Mg_2Si and the white one was multicomponent (Al, Si, Sc) phase.

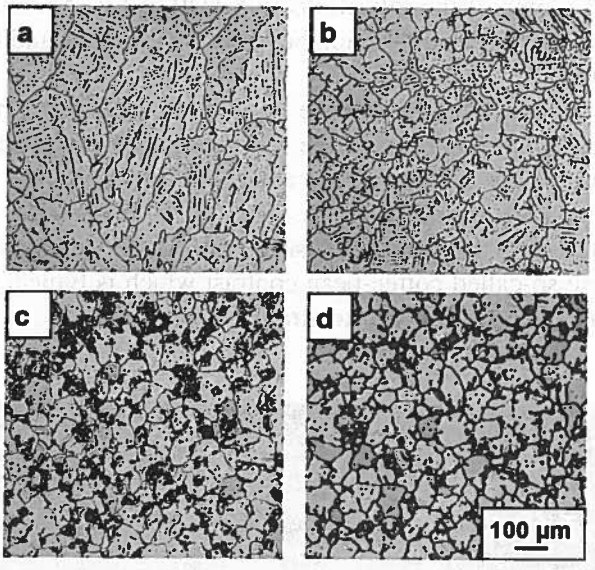

Fig. 2. Optical micrographs of as cast alloy A (Al-1% Mg-0.6% Si-0.4% Sc) (a, b) and alloy B (Al-1% Mg-0.6% Si-0.4% Sc-0.2% Zr) (c, d). The regions near the walls of the mould are shown in (a, c), in comparison with the centre of the ingots (b, d)

The grain refinement in alloy B is achieved by the formation of a large number of the $L1_2$-Al_3Sc crystals which precipitate as primary intermetallic particles in the melt on solidification and form nuclei of the α (Al) solid solution. The effectiveness of the grain refinement of the Al_3Sc phase is attributed to the similarity of the crystal lattices of the nuclei and the matrix (discrepancy between lattice parameters is about 15%). The example of the primary particle that form in the alloy B (annealed at 350°C/0.5h and 540°C/0.5h) is shown in TEM bright- and dark-field images in Fig. 4. The primary particle is surrounded by very fine spherical precipitates which nucleated from the supersaturated solid solution during annealing. In the corresponding diffraction pattern the Al_3Sc reflections are in superlattice positions in agreement with $L1_2$-type structure (lattice constant a = 0.410 nm, similar to that of aluminium). Dark-field image obtained from the superlattice reflection confirms that primary particles as well as secondary precipitates are Al_3Sc phase. A precipitate free zone appeared around the primary Al_3Sc particle and it suggests that the growth of those particles was continued in the solid state on the expense of some solute from the surrounding matrix.

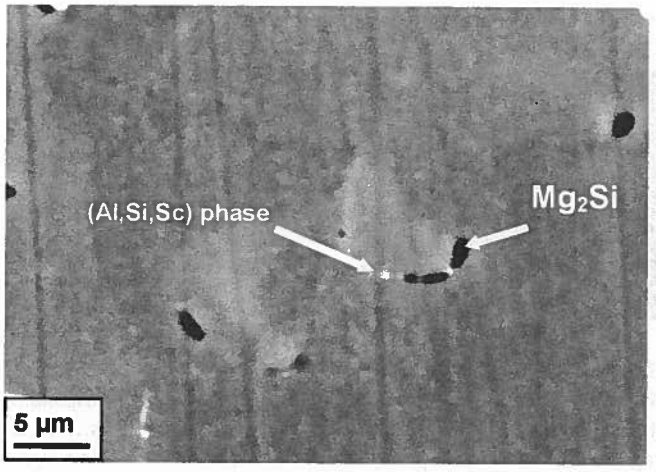

Fig. 3. SEM image of the as cast alloy B

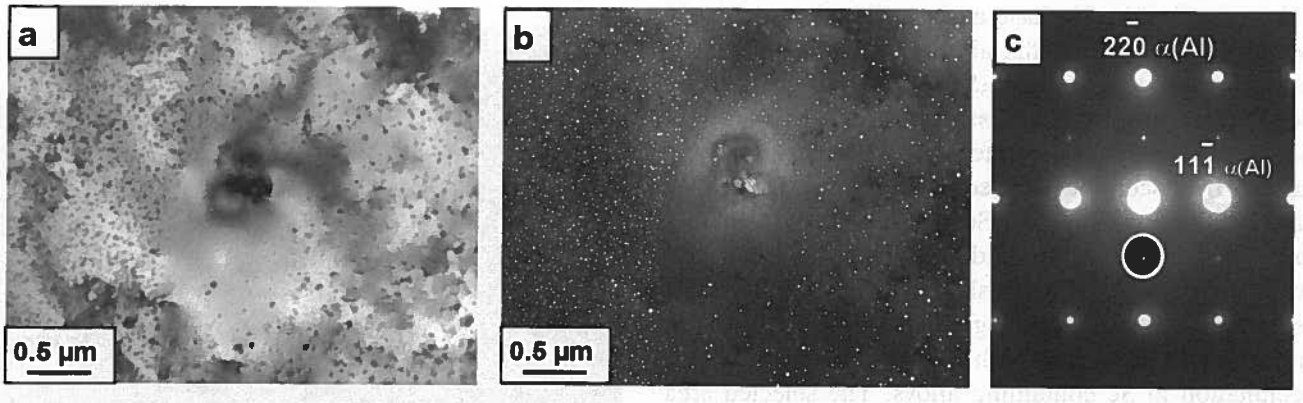

Fig. 4. TEM (a) bright- and (b) dark-field images and (c) corresponding diffraction pattern of the alloy B (Al-1% Mg-0.6% Si-0.4% Sc-0.2% Zr) annealed at 350°C/0.5 h and at 540°C/0.5 h, taken along the [112] α (Al) zone axis. The reflection used for dark-field imaging is marked in (c) by circle

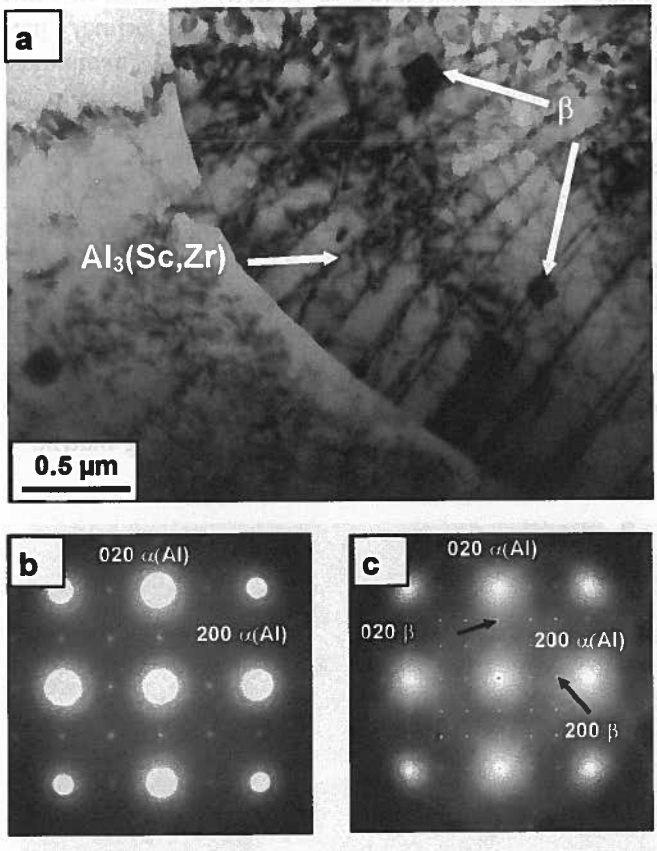

Fig. 5. (a) TEM bright-field image of alloy B (Al-1% Mg-0.6% Si-0.4% Sc-0.2% Zr) annealed at 350°C/0.5 h and corresponding diffraction patterns taken along the [001] α (Al) zone axis from the region of discontinuous precipitation (b) and from the cubic-shape β phase (c)

During the first step of annealing at 300/350°C the following processes took place: the partial dissolution of the eutectic Mg_2Si phase and precipitation of Mg_2Si and Al_3Sc phases from the aluminum solid solution. It has been reported that the Al_3Sc precipitates can form in two different ways: (i) supersaturated solid solution decomposes to less supersaturated solid solution and Al_3Sc particles by discontinuous precipitation behind a moving grain boundary and (ii) Al_3Sc phase nucleates directly from the supersaturated solid solution [5]. In Fig. 5a. the TEM image shows a fan-shaped array of precipitates inside the part of the right grain. This is a typical arrangement for precipitates which form by discontinuous precipitation in Sc containing alloys. The selected area diffraction pattern (SADP) from this region contains the superlattice reflections in the Al_3Sc positions (see Fig. 5b.). The cubic shape particles are also visible in both grains in Fig. 5a. The additional reflections in the SADP obtained from one selected cuboidal particle (Fig. 5c.) can be indexed as β-Mg_2Si transition phase (Fcc, a = 0.633 nm) relating to the matrix with the cube-cube orientation relationship (100)β || (100)Al, (010)β || (010)Al [12]. Some of the reflections in SADP in Fig. 5c. arose from the double diffraction between the particles and the matrix.

In another area of the same specimen the small spherical precipitates of the Al_3Sc were observed apart from to the needles lying along <001> directions of the α (Al) matrix (Fig. 6). The TEM image (Fig. 6) shows that the densily distributed Al_3Sc precipitates cause so-called coffee-bean contrast which is typical for coherent particles, due to strain field contrast.

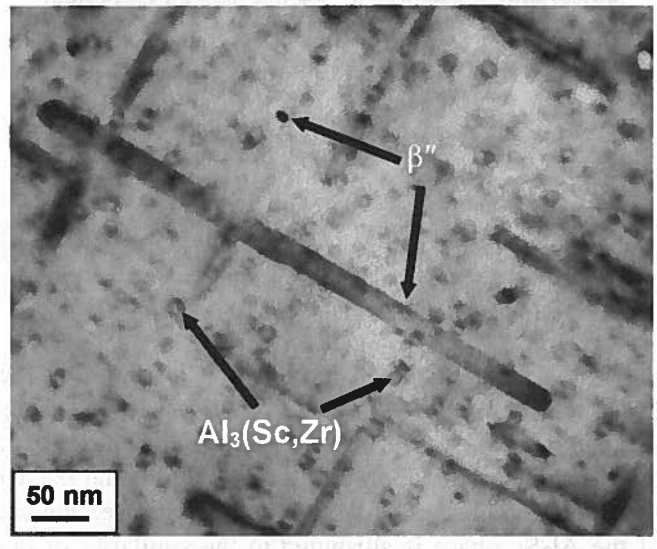

Fig. 6. TEM bright-field image of alloy B (Al-1% Mg-0.6% Si-0.4% Sc-0.2% Zr) annealed at 350°C/0.5 h taken near the [001] α(Al) zone axis

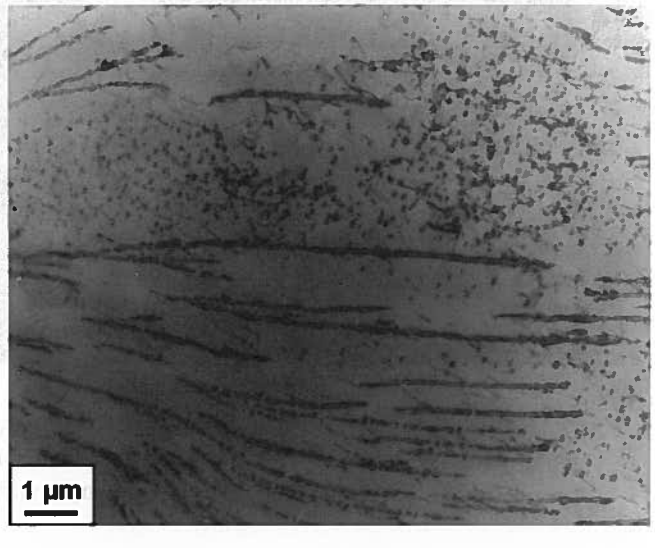

Fig. 7. TEM bright-field image of alloy A (Al-1% Mg-0.6% Si-0.4% Sc) annealed at 300°C/0.5h + 540°C/0.5h taken along the [001] α (Al) zone axis

After subsequent annealing at 540°C followed by water quenching to water, the β'' and β precipitates completely dissolved while the Al_3Sc particles grew. The TEM image presented in Fig. 7. shows the area of the alloy A containing discontinuous precipitations of the Al_3Sc phase as well as the region containing spherical particles of Al_3Sc phase.

It was observed that Sc containing phase (see Fig. 2) did not dissolve during annealing, performed in the temperature range 300-540°C. The Sc-rich particles situated on the grain boundary are presented in TEM bright-field image (Fig. 8). The EDX spectrum and SADP from one separate particles (marked by an arrow in Fig. 8) allowed to identify it as a tetragonal V-$AlSi_2Sc_2$ phase (a = 0.6597 nm, c = 0.3994). It was observed that the spherical precipitates of the Al_3Sc phase formed also inside the grains of the aluminum solid solution. A precipitate free zone along the grain boundary, which contain Sc-rich particles are also visible.

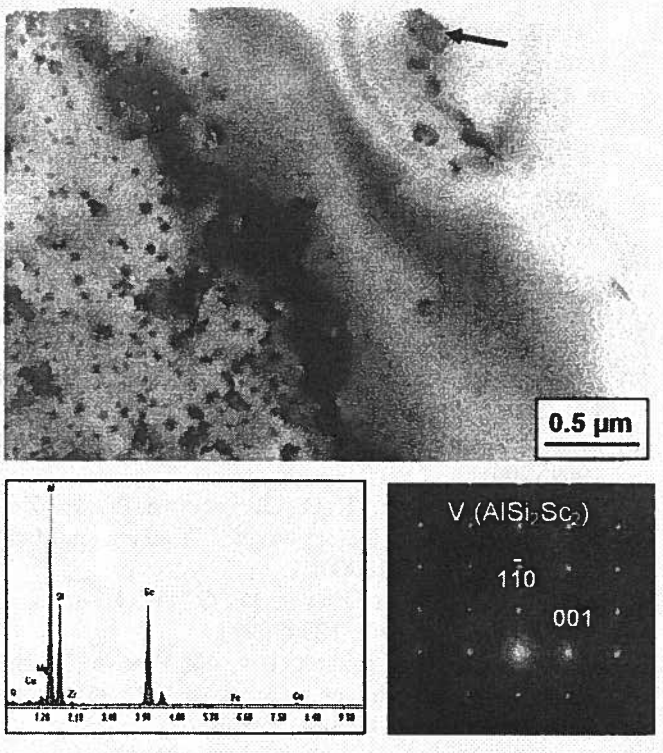

Fig. 8. TEM bright-field image of alloy A (Al-1% Mg-0.6% Si-0.4% Sc) annealed at 300°C/0.5h + 540°C/0.5h and EDX spectra and the SADP obtained from the particle marked by arrow

Dark-field TEM image of alloy A containing 0.4% Sc of the [001] α(Al) zone axis orientation show Al_3Sc particles about 70-80 nm in size, uniformly distributed in the matrix (Fig. 9a). The Al_3Sc reflections are in superlattice positions in agreement with the $L1_2$ structure as can be seen in the corresponding diffraction pattern inserted in Fig. 9a. As have been reported in [13], the precipitates in alloy A partially lose of coherency with the matrix and interfacial misfit dislocation are frequently seen around them. In alloy B with Sc and Zr addition, the precipitates are smaller (Fig. 9b), which was expected from the known stabilizing effect of Zr on Al_3Sc particles [4, 5]. The precipitates are 10-30 nm in size, and are fully coherent with the matrix [13].

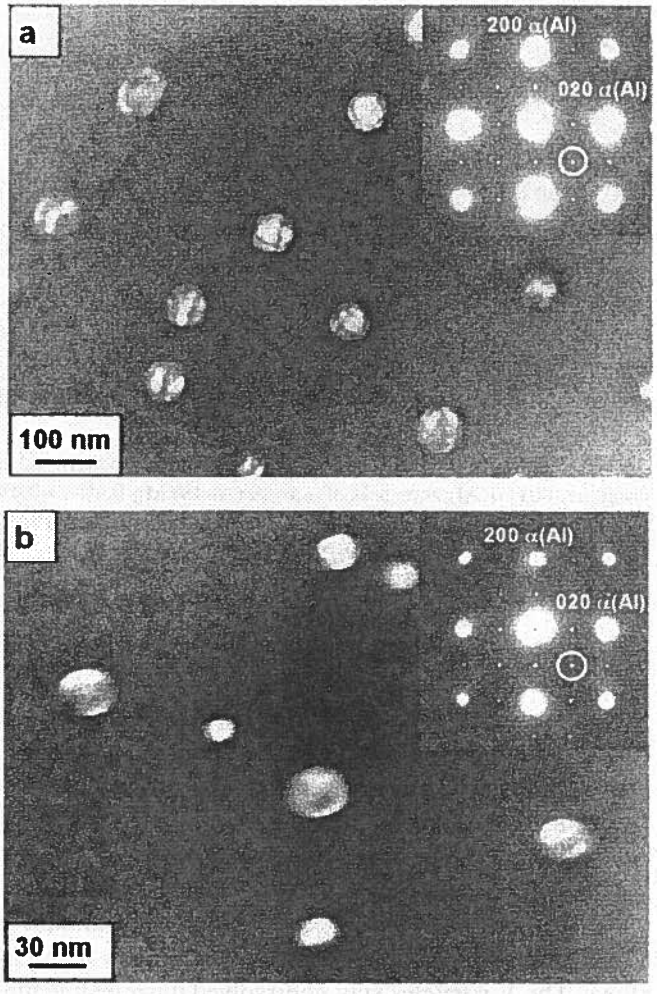

Fig. 9. TEM dark-field images and corresponding diffraction patterns as inserts of (a) alloy A (Al-1% Mg-0.6% Si-0.4% Sc) annealed at 300°C/0.5 h and at 540°C/0.5 h and (b) alloy B (Al-1% Mg-0.6% Si-0.4% Sc-0.2%Zr) annealed at 350°C/0.5 h and at 540°C/0.5 h, taken along the [001] α(Al) zone axis. The reflections used for dark-field imaging are marked by circles in the SADP's

The increase of the hardness of both alloys, detected after additional ageing at 165°C [11], is caused by the precipitation of the β'' phase which is the main strengthening phase in 6000 series alloys. A TEM microstructure and a corresponding diffraction pattern of a peak-hardened alloy containing 0.4 wt.% Sc are presented in Fig. 10. The Al_3Sc particles (whose size does not change after ageing at 165°C) co-exist with needle-like β'' precipitates. The presence of the β'' phase was confirmed by spots within the streaks along the <001> di-

rections on the diffraction pattern. The streaks arise from the shape effect of the two variants of needles lying perpendicular to the electron beam. The β'' precipitates are distributed nearly homogeneously in the matrix and no precipitate-free zone around Al_3Sc particles was found. This suggests that Al_3Sc particles contain neither Mg nor Si, which are the components of β'' precipitates.

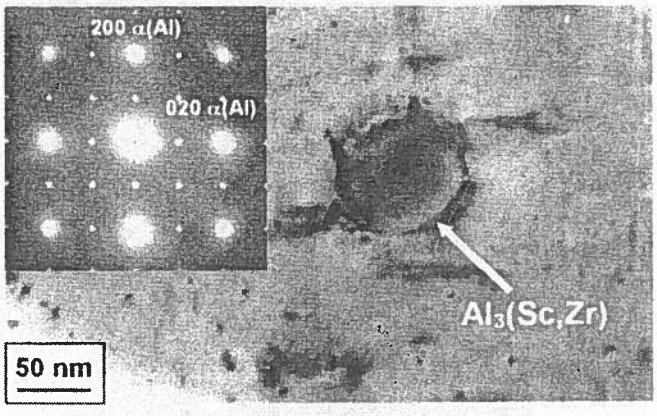

Fig. 10. TEM image and corresponding diffraction pattern taken along the [001] α(Al) zone axis of alloy A (Al-1% Mg-0.6% Si-0.4% Sc) annealed at 300°C/0.5h + 540°C/0.5h and aged for 6h at 165°C

4. Conclusions

1. The addition of 0.4 wt% Sc+0.2 wt% Zr have a strong grain refining effect in as cast condition and eliminates the dendrites. The grain refinement is achieved by the formation of a large number of the $L1_2$-Al_3Sc crystals which precipitate as primary intermetallic particles in the melt on solidification.

2. The Mg_2Si phase coexist with small amount of V-$AlSi_2Sc_2$ phase formed at the grain boundary in as cast alloys. The V particles stay undissolved during annealing at 300-540°C.

3. The Al_3Sc phase precipitated both by discontinuous (in the form of the fan-shaped array of precipitates) and by continuous mode (as small spherical particles, coherent with the matrix) during annealing at 300/350°C the. The β'' needles lying along <001> directions of the α(Al) matrix and cuboidal particles of the β-Mg_2Si transition phase were also observed.

4. After subsequent annealing at 540°C $L1_2$-Al_3Sc spherical precipitates about 60-70 nm in size in alloy A are semicoherent with the matrix. The addition of Zr limits the size of Al_3(Sc, Zr) precipitates to about 10-30 nm, and these precipitates are fully coherent with the matrix.

5. After additional ageing at 165°C, the needle-like precipitates of the metastable $\beta''(Mg_2Si)$ phase leads to an increase of hardness of both alloys.

Received: 20 September 2006.

Acknowledgements

The author acknowledge the financial support of the State Committee for Scientific Research in Poland (Research Project 4T08B 008 24).

REFERENCES

[1] J. P. Lynch, L. M. Brown, M. H. Jacob, Acta Metall. **30**, 1389 (1982).
[2] K. Matsuda, Y. Sakaguchi, Y. Miyata, Y. Uetani, T. Sato, A. Kamio, S. Ikeno, J. Mat. Sci. **35**, 179 (2000).
[3] D. J. Chakrabarti, D. E. Laughlin, Progress in Materials Science **49**, 389 (2004).
[4] L. S. Toropova, D. G. Eskin, M. L. Kharakterova, T. V. Dobatkina, Advanced Aluminum Alloys Containing Scandium, Gordon and Breach Science Publishers (1998).
[5] J. Royset, N. Ryum, Intern. Mater. Rev. **50**, 19 (2005).
[6] A. F. Norman, P. B. Prangnell, R. S. McEwen, Acta Mater. **46**, 5715 (1998).
[7] G. Novotny, A. J. Ardell, Mater. Sci. Eng. **A318**, 144 (2001).
[8] E. A. Marquis, D. N. Seidman, Acta Mater. **49**, 1909 (2001).
[9] V. G. Davydov, T. D. Rostova, V. V. Zakharov, Yu. A. Filatov, V. I. Yalagin, Mater. Sci. Eng. **A280**, 30 (2000).
[10] M. L. Kharakterova, D. G. Eskin, L. L. Rokhlin, Metally **1**, 123 (1997).
[11] L. Lityńska, J. Dutkiewicz, Proc. of International Conf. "Aluminium in Transport" 22-25 October 2003, Tomaszowice-Krakow, 175 (2003).
[12] Y. Ohmori, L. C. Doan, Y. Matsuura, S. Kobayashi, K. Nakai, Mat. Trans. **42**, 2576 (2001).
[13] L. Lityńska, J. Dutkiewicz, H. Heinrich, G. Kostorz, Acta Metallurgica Slovaca **10**, 514 (2004).